Dalton Transactions

Accepted Manuscript

ROYAL SOCIETY OF CHEMISTRY

www.rsc.org/dalton

Cite this: DOI: 10.1039/c0xx00000x

www.rsc.org/xxxxxx

ARTICLE TYPE

Controlled *in-situ* fabrication of Ag_2O/AgO thin films by a dry chemical route at room temperature for hybrid solar cells

Jie Wei[1,2], Yan Lei[1], Huimin Jia[1], Jiamei Cheng[1,2], Hongwei Hou[2]*, Zhi Zheng[1]*

[1]Key Laboratory of Micro-Nano Materials for Energy Storage and Conversion of Henan Province and Institute of Surface Micro and Nano Materials, Xuchang University Henan 461000, China
[2]The College of Chemistry and Molecular Engineering, Zhengzhou University Zhengzhou 450000, China

Received (in XXX, XXX) Xth XXXXXXXXX 20XX, Accepted Xth XXXXXXXXX 20XX
DOI: 10.1039/b000000x

Silver oxides (Ag_2O and AgO) have attracted increasing attention as potential solar cell materials for photovoltaic devices due to their ideal bandgap and non-toxicity. In order to eliminate the complicated synthesis and harsh reaction conditions (e.g. high temperature, high vacuum, high energy input, electron beam instrumentation) required by most synthetic strategies, we developed a very facile dry chemical approach to directly prepare Ag_xO species on ITO substrate by taking advantage of a UV-O_3 surrounding in a controlled way. We systematically investigated the effects of relative humidity, reaction temperature, and silver deposition technique on the formation of silver oxide (AgO or Ag_2O) thin films. A possible synthetic mechanism for the formation of AgO and Ag_2O is proposed. More importantly, we have designed and successfully fabricated a novel inorganic hybrid Ag_2O/Bi_2O_3 heterojunction thin film for the first time which exhibits significantly improved photocurrent compared with pure Bi_2O_3 film.

1. Introduction

To maximize the energy conversion efficiency of photovoltaic cells (PVs), PV light absorption materials must have an appropriate bandgap to harvest the full spectrum of sunlight. Theoretically, a bandgap of 1.4 ~ 1.5 eV is ideal to match the solar spectrum[1]. Much effort has been devoted to finding suitable light absorption materials in the past decade. For example, CdTe, Cu(In,Ga)Se_2 (CIGS), and Cu_2ZnSnS_4 (CZTS) are promising absorption materials for light harvesting[2,3,4]. However, these materials have several drawbacks including toxicity, low elemental abundance, and/or complicated synthesis processes. In recent years, Ag_2O and AgO have attracted increasing attention as potential light absorption materials for photovoltaic cells due to their ideal bandgap and non-toxicity[5]. Furthermore, Ag_2O and AgO are the most thermodynamically stable compounds within the silver oxide family, which also includes Ag_2O_3, Ag_3O_4 and Ag_4O_3. In particular, Ag_2O is an intrinsic p-type semiconductor with a suitable bandgap of 1.46 eV and is environmentally friendly[5]. Therefore, Ag_2O is potentially advantageous as a light absorption material, especially in terms of having a bandgap within the ideal energy range of 1.4 ~ 1.5 eV. Ag_2O, which has the same crystallographic structure as Cu_2O (cubic cuprite), has previously been used as a cocatalyst[6], thin film sensor[7], optical data storage material[8], and as a cathode in the zinc-silver oxide battery[9]. In contrast, AgO is an interesting compounds in that the oxidation states of the elements are not obvious based on the chemical formula. In fact, AgO is a mixed valence compound which can be explicitly written as $Ag^{I}Ag^{III}O_2$. AgO has the same crystal structure as CuO, but is less stable[10].

Silver oxide (Ag_2O) particles have been successfully synthesized for over 100 years. In 1902, Kohr and coworkers[11] synthesized Ag_2O particles by mixing solutions of silver nitrate and barium hydroxide. Ag_2O nanoparticles were also obtained using a similar method. Other Ag_2O morphologies have also been obtained[12] with a wet-chemical approach using $AgNO_3$, $NH_3{\cdot}H_2O$ /NH_4NO_3 and NaOH as reactants to yield structures such as cubes, octahedra, truncated cubes/octahedra, and hexapods. Douglas B.Chrisey[13] et al. fabricated Ag_2O pyramids, triangular plates, pentagonal rods, and bars by pulsed exciter laser ablation of an Ag target. Several other techniques have also been applied

to synthesize silver oxide including thermal or anodic oxidation[14], chemical vapor deposition[15], anodic electrodeposition[5,16], and RF magnetron sputtering[17]. The synthetic strategies listed above have considerable drawbacks including the need for high temperatures, pressures, and vacuum conditions, resulting in high energy consumption. There are few reports related to the direct growth of Ag_2O or AgO thin films until now, except that Bowmaker and coworkers obtained silver oxide thin films by reacting silver foil with ozone at 300 K[18]. Here, we designed a very facile and environmentally friendly approach for controlled *in-situ* growth of Ag_2O and AgO thin films using a direct solid-state elemental reaction strategy. Compared with the previous wet chemical routes, pure Ag_2O and AgO thin films could be directly prepared on ITO or Bi_2O_3 surface for further construction of bulk-heterojunctions.

To our knowledge, synthesizing Ag_2O or AgO thin films for hybrid solar cell fabrication has not been reported previously. By selecting proper n-type substrate materials, such as Bi_2O_3 and WO_3 that can match the energy level of p-Ag_2O, these results are promising for the development of p-Ag_2O based bulk-heterojunctions for the next generation of hybrid solar cell.

2. Experimental section

2.1 Sample preparation

The patterned ITO substrate was cleaned by ultrasonic treatment in detergent solution for 20 minutes, then the ITO substrate was treated with $NH_3{\cdot}H_2O$:H_2O_2:H_2O (volume ratio, 1:2:5) mixed solution at 80^{o}C for 30 minutes, at last it was cleaned with distilled water two times and dried at 80^{o}C for 4h for use. A 100 nm silver layer was then coated onto the clean ITO substrate under Ar atmosphere by magnetron sputtering of an Ag target (99.99%) in the presence of a mask. The base pressure in the chamber was kept below 1.0×10^{-4} mbar, and sputter deposition was carried out under a working pressure of 7×10^{-3} mbar at a power of 1000 VA. The silver film thickness was detected by a film thickness monitor (FTM). The silver films on the ITO substrates were placed in a UV-O_3 instrument (PSD-UV4, Navascan Technologies, Inc.), which can irradiate with two wavelengths of light (185 nm and 254 nm). A suitable amount of O_2 was added into the chamber from the inlet valve. Finally, the air inlet and outlet to the chamber were sealed, and after 1 h a black Ag_2O thin film on the ITO substrate was obtained. In a typical synthesis, the reaction temperature and relative humidity were kept at about 25^{o}C and 60%, respectively. In order to study how temperature and humidity affect Ag_xO semiconductor thin film morphology, size, crystal phase, and crystal growth, parallel experiments were also carried out at(0 ^{o}C, 30 %), (10 ^{o}C, 40 %), (20 ^{o}C, 50 %) and (35 ^{o}C, 90 %).

Ag_2O thin films were also synthesized on ground-glass and silicon wafer substrates by a similar method.

2.2 Characterization

Apparatus A Bruker D8 ADVANCE X-ray diffractometer was employed to characterize the structure of the samples with nickel-filtered Cu-Ká radiation, 40 kV, 40 mA and a scanning rate of 0.02^o s^{-1} with the 2θ range from 20 to 80^o. SEM images were obtained from a Zeiss EVO LS-15 scanning electron microscope, and the accelerating voltage is 15 kV. The selected area electron diffraction (SAED) patterns, transmission electron microscopy (TEM), and high-resolution transmission electron microscopy (HRTEM) data were recorded by a JEM-2100 transmission electron microscope, and the accelerating voltage of TEM is 200 kV. The UV-vis absorption spectrum was collected with a Carry 5000 UV-vis spectrometer. X-ray photoelectron spectroscopy (XPS) data were acquired on a Thermo ESCALAB 250 X-ray photoelectron spectrometer with an Al-Ká excitation source (1486.6 eV). The carbon C 1s line with position at 284.8 eV was used as a reference to correct the charging effect. Filed-emission scanning electron microscopes (FESEM) images were obtained using a Hitachi S-4800 SEM (operated at 10 kV).

3. Results and Discussion

Many researchers have proposed wet chemical approaches for the fabrication of Ag_2O. The basic principle is to break down silver ammonium ions ($Ag(NH_3)_2^+$) in strong alkaline solution to yield AgOH. Since AgOH is not stable at room temperature, it decomposes to yield Ag_2O. In contrast to solution-based fabrication, our reaction design is based on a completely different dry chemical approach. The most important factors for this method are temperature and relative humidity. We found that adjustments to the temperature and relative humidity can drive the formation of two different silver oxides (either AgO or Ag_2O).

There are three oxidizing species in the reaction process including O_2, O_3 and O. The impact of the three oxidizing agents

on the thermodynamics of the system is a dynamic balancing process[19]. Atomic oxygen (O) has a total of eight electrons with an electronic configuration of $1s^2 2s^2 2p^4$; there are two different states of atomic oxygen according to Pauli Exclusion Principle and Hund's rule, which are the ground state and excited state. The excited state of atomic oxygen has one empty 2p orbital, and is electrophilic and prone to undergo bond forming addition reactions. Additionally, the radiolysis of water (reaction (3)) yields hydroxyl radicals (·OH) that have higher oxidation potentials than other kind of oxides. Therefore, active oxygen atoms (O) and hydroxyl radicals (·OH) play key roles in the reaction process for Ag_xO.

$$2Ag + O \rightarrow Ag_2O \quad (1)$$

$$Ag_2O + O \rightarrow Ag_2O_2\ (AgO) \quad (2)$$

$$O + H_2O \rightarrow H_2O_2 \rightarrow 2\ \cdot OH \quad (3)$$

$$Ag + \cdot OH \rightarrow 2\ AgOH \rightarrow Ag_2O + H_2O \quad (4)$$

Active oxygen atoms make contact and react quickly with elemental silver thin films when the relative humidity is low (≦ 40%), because (i) active oxygen atoms move fast and (ii) the surface of thin film has a very thin layer of water molecules. The reaction of active oxygen atoms with metallic silver is shown in reaction equation (1) to yield Ag_2O, which is conformed to Li and colleagues[20]. The reactive oxygen atoms continue to interact and react with the generated Ag_2O to yield a brownish black AgO thin film, as shown in reaction equation (2). As Waterhouse pointed out, the as-prepared Ag_2O further react with active atoms to form a mixed Ag_2O_2 (AgO)[18]. In contrast, when the relative humidity is high (≧65%), oxygen atoms move slower and the surface of the metallic silver thin film is covered with a larger barrier of water molecules that hinders active oxygen atoms from reacting with the elemental silver film. Therefore, under such high humidity condition, active oxygen atoms that can penetrate to react with elemental silver atoms are limited and only reaction (1) could be conducted to form pure Ag_2O thin films. There are not enough reactive oxygen atoms to further conduct reaction (2) and generate AgO films.

Alternatively, when the relative humidity is less than 40%, active oxygen atoms is more dominant than ·OH and thus react rapidly with elemental silver surface according to reaction (1), the Ag_2O was further oxidized by reactive oxygen atoms to generate AgO according to reaction (2)[18]. Even reaction (3)[21] and (4)[22] can occur, the as-generated Ag_2O will inevitably be further oxidized by successive reactive oxygen atoms to produce AgO finally according to reaction (2). When the relative humidity is in the range of 40% ~ 65%, the amounts of O and ·OH are comparable, such that both AgO and Ag_2O thin films are likely to be formed according to reaction (1), (2) and (4). In contrast, when the relative humidity is as high as ≧65％, water molecules are abundant and reaction (3) proceeds extensively. In this case, since ·OH is more dominant than O, an Ag_2O instead of AgO thin film is obtained.

To understand the compositions and structures of the as-prepared silver oxide thin films, we carried out X-ray diffraction (XRD). Fig.1a shows the XRD patterns of AgO samples prepared under varying temperature and relative humidity conditions, while all other reaction conditions are kept constant. All the diffraction peaks match AgO, which can be indexed with the literature value of hexagonal-phase AgO (JCPDS No.89–3081), with lattice constants of 2.621 Å and 2.413 Å. No diffraction peaks from impurities are detected, except for the peak assigned to the ITO substrate. This result indicates that these films are composed of highly pure AgO particles. From curves (2) and (1), we learn that the (002) and (-311) peaks begin to emerge as relative humidity increases. The (200) and (111) peaks also become stronger under higher humidity conditions. Comparing curves (3) with (2), the (200), (111), and (-202) peaks become quite strong with increasing temperature. These results demonstrate that there is an optimal range of temperature and relative humidity for the synthesis of pure AgO thin films. We adopted a similar approach to synthesize Ag_2O thin films by further increasing the relative humidity compared to AgO thin film fabrication conditions.

The effect of the substrate on silver oxide thin film formation was also tested using different basal silver materials. The first silver/ITO substrate was obtained by magnetron sputtering in the present of a mask (b (1)) with a chamber pressure of approximately 7.0×10^{-3} mbar; the purity of silver target used was 4N. The other silver/ITO substrate was obtained by thermal evaporation deposition (b (2)), with the chamber pressure set at around 3.0×10^{-4} mbar. The purity of the filamentary silver we used is 4N. Subsequently, silver oxide thin films were synthesized under conditions of 28°C and 70% relative humidity on the different basal silver substrates. Fig.1b shows the XRD patterns of the Ag_2O samples with different basal silver materials. From Fig.1b, we see that the relative intensity of

(111) and (200) peaks are dramatically different based on the choice of silver/ITO substrate, indicated that the advantageous crystal growth faces of Ag_2O thin films could be well controlled using the method we developed by choosing appropriate substrate.

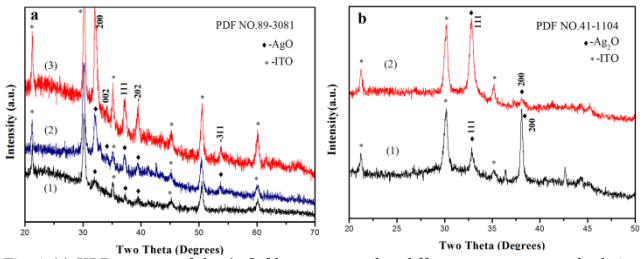

Fig. 1 (a) XRD patterns of the AgO film as-prepared at different temperature and relative humidity ((1) 12°C, 30%; (2) 12 °C, 60% and (3) 22 °C, 60%)). (b) XRD patterns of the Ag_2O film as-prepared at different silver substrates ((1) silver substrate obtained by magnetron sputtering and (2) silver substrate obtained by thermal evaporation deposition).

Fig. 2 shows the XRD patterns of the samples obtained under different relative humidity conditions. At 30% relative humidity, all the diffraction peaks match AgO, except for the peak assigned to the ITO substrate. The (111) peak of Ag_2O arises when the relative humidity increases to 40%. At 60% relative humidity, the (200), (002) and (-202) peaks of AgO begin to disappear, while the (111) and (200) peaks of Ag_2O become stronger. For relative humidity higher than 60%, diffraction peaks from AgO completely disappear, and all the peaks observed can be assigned to Ag_2O. Thus we find that, our dry chemical approach promotes the formation of silver oxide thin films composed of a mixture of AgO and Ag_2O when the relative humidity is 40% ~65%, and pure AgO films are synthesized when the relative humidity is equal to or less than 40%. Likewise, pure Ag_2O films can only be formed under relatively humidity higher than 60%. The relative humidity is a key factor in determining the final product and purity of Ag_xO species. By tailoring the experimental conditions, we can specifically synthesize the desired product.

Differences in film morphology are observed and recorded in Fig. 3 as a result of relative humidity during silver oxide film fabrication. Fig. 3a-c shows the typical morphologies of the AgO films obtained under relative humidity conditions of 30%, 50%, and 60%. AgO films were made of uniform spherical nanoparticles when the relative humidity was 30%, 50%, and 60%, respectively (Fig 3a-c). Fig. 3e shows the low-magnification TEM of AgO nanoparticles; the average diameter of the AgO nanoparticles was ~20 nm. Fig. 3d shows the HRTEM of the AgO nanoparticles, demonstrating the well-resolved 2D lattice fringes with a lattice spacing of 2.41 Å, which corresponds to the (200) plane of the AgO monocrystal. At relative humidity levels of 65% and 90%, Ag_2O films were obtained and their morphologies are illustrated in Fig. 4a-b. From Fig. 4a, we can clearly see that uniform spherical Ag_2O nanoparticles were obtained when the relative humidity was 65%. However, the substrates could not be fully covered with Ag_2O nanoparticles at 65% relative humidity. Dense film coverage and uniform Ag_2O nanoparticles were obtained at a relative humidity of 90% on ITO substrates (Fig. 4b). Fig. 4c-d shows the HRTEM of Ag_2O nanoparticles prepared on different silver/ITO substrates (silver film was obtained by magnetron sputtering (c) and thermal evaporation deposition (d)). All the well-resolved 2D lattice fringes in Fig. 4c and Fig. 4d have a lattice spacing of 2.35 Å and correspond to the (200) plane of the Ag_2O monocrystal. The low-magnification TEM of Ag_2O (Fig. 4e) shows that the average diameter of Ag_2O nanoparticles was also ~20 nm.

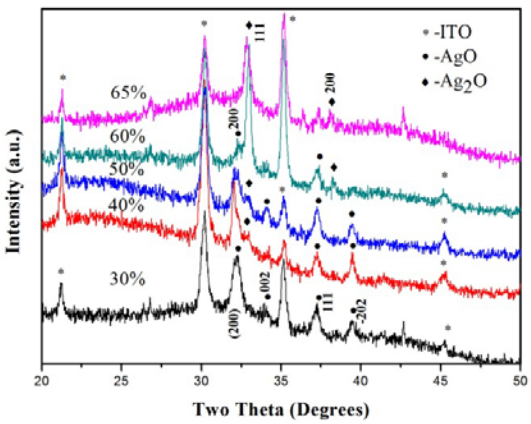

Fig. 2 XRD patterns of the as-prepared samples at 20°C for different relative humidity (30%, 40%, 50%, 60% and 65%).

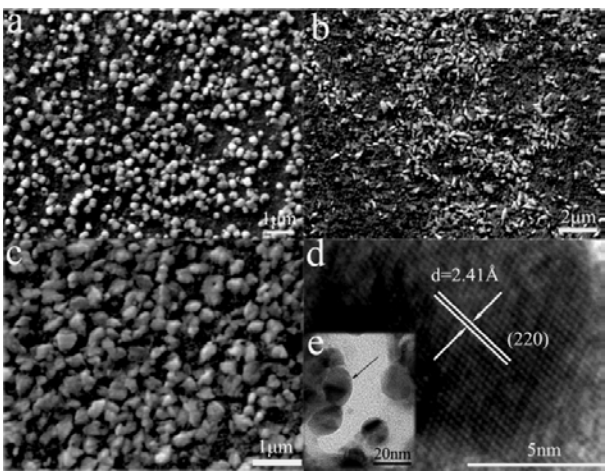

Fig. 3 SEM images of AgO thin films were obtained at different relative humidity 30% (a), 50% (b) and 60% (c). HRTEM (d) and TEM (e) images of the AgO nanoparticles from the AgO thin films as-prepared at relative humidity 30%.

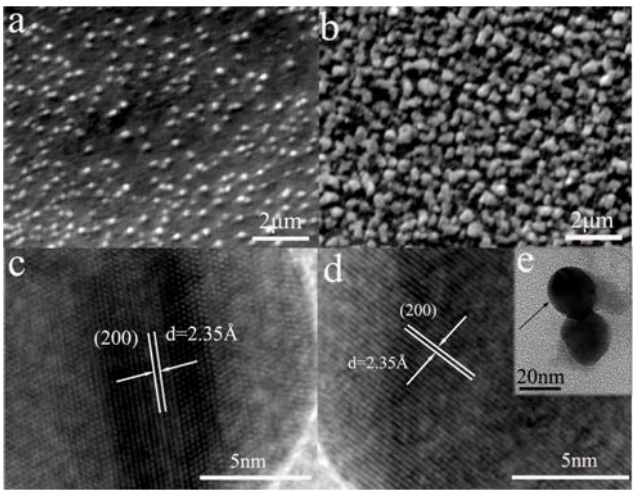

Fig. 4 SEM images of Ag_2O films were obtained at 28 °C and relative humidity 65% (a) and 90% (b) for 1 hour on silver/ITO substrates (silver film was obtained by magnetron sputtering). The HRTEM images of the Ag_2O nanoparticles from the Ag_2O film as-prepared on different silver/ITO substrates (silver film was obtained by magnetron sputtering (c) and thermal evaporation deposition (d and e)).

In order to further confirm the compositions and chemical species/states of Ag_2O and AgO, we carried out X-ray photoelectron spectroscopy (XPS) on our samples. Fig. 5 shows the XPS spectra of the as-prepared Ag_2O (60nm in thickness, 28 °C, relative humidity of 80%) and AgO films (60nm in thickness, 22 °C, relative humidity of 50%), Fig. 5a shows the XPS core level spectrum of O1s for Ag_2O. The binding energy (BE) of the O 1s peak is 531.5 eV. The BE of the O 1s peak obtained from our Ag_2O sample is shifted by 0.3 eV compared to reports by Gar B. Hoflund[23]. The Ag 3d peaks of the sample are presented in Fig. 5b, which shows Ag splitting into two peaks, Ag $3d_{5/2}$ and Ag $3d_{3/2}$, centered at 368.5eV and 374.5eV, respectively. This confirms that the as-prepared sample in Fig.5a is Ag_2O since Ag^+ has a splitting energy of 6.0 eV[24]. The XPS core level spectrum of O 1s and Ag 3d for AgO are shown in Fig. 5c-d, respectively. Hoflund and co-workers[25,26] found that the binding energies of Ag $3d_{5/2}$ in Ag, Ag_2O, and AgO were 368.0, 367.7, and 367.2 eV, respectively. From Fig. 5b and Fig. 5d, we see that the binding energy of Ag $3d_{5/2}$ appears at 368.5 eV and 368.3 eV, a shift of 0.5 eV and 0.3 eV, respectively, compared to Ag metal (BE = 368.0 eV). Overall, XPS shows that, relative to the metallic state, the BE of the Ag 3d peaks shift 0.5 and 0.3 eV for AgO and Ag_2O, respectively. A positive BE shift in the Ag core-level peaks is that expected between a metal and its oxides. Such a positive BE shift agrees well with Hofund's report[25], in which Ag(I) and Ag(III) could not be resolved by XPS. From Fig. 5a and 5c, we found that O1s of both Ag_2O and AgO has a higher binding energy of 531.5 eV and 531.2 eV respectively, because a mixture of O and ·OH may exist in the subsurface of Ag_2O and AgO thin films according to Hofund[25].

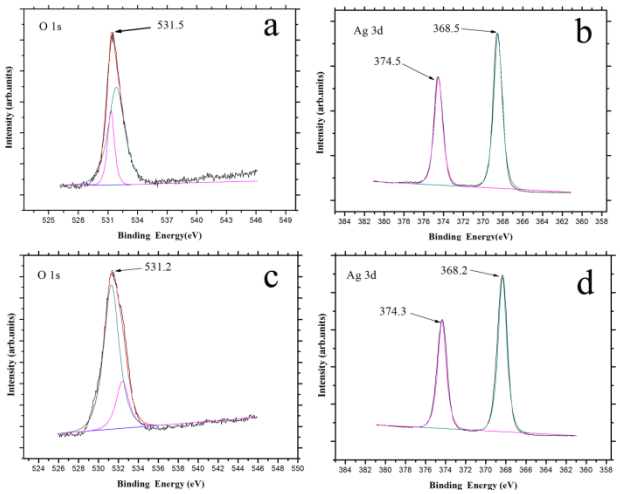

Fig. 5 (a) high resolution XPS spectrum of O 1s, (b) high resolution XPS spectrum of Ag3d for Ag_2O as-prepared at 28 °C and 80%, (c) high resolution XPS spectrum of O 1s and (d) high resolution XPS spectrum of Ag3d for AgO as-prepared at 22 °C and 50%.

The photocurrent generated from the electron-hole separation, and a suitable p-n heterojunction has the ability to enhance the charge separation, as a result the photocurrent density will be increased. For example, the composite thin $BiVO_4/WO_3$ films showed a higher photocurrent density than pure $BiVO_4$ or WO_3 thin films[27]. Ag_2O is a p-type semiconductor with an ideal bang gap, and the energy level of valence band and conduction band matched well with the n-type semiconductor Bi_2O_3, and a suitable band alignment p-n junction can be formed at the interface of the two materials. The corresponding energy levels and charge-transfer processes occurring within the Bi_2O_3/Ag_2O hybrid thin film were depicted in Fig. 6.

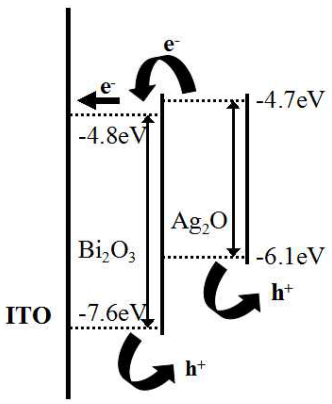

Fig. 6 Schematics of the potential energy diagram for the Ag_2O/Bi_2O_3 heterojunction composite thin film electrode.

To test the photovoltaic performance of the Bi_2O_3/Ag_2O hybrid thin film electrode, a 200 nm metal bismuth was deposited on the as-prepared Ag_2O films by magnetron sputtering. Then Bi/Ag_2O/ITO substrates were placed in a muffle furnace at 150°C for four hours and cooled naturally to room temperature, resulting in Bi_2O_3/Ag_2O hybrid thin films on ITO substrates. XRD patterns of pure Bi_2O_3 thin films and Bi_2O_3/Ag_2O composite thin films are shown in Fig. 7a. The diffraction peaks of bismuth oxide were marked with * in Fig. 7a-1, and all these diffraction peaks can be indexed well with the information of standard Bi_2O_3 (JCPDS No.29-236). The diffraction peaks (111) and (200) came from the monoclinic-cubic Ag_2O (JCPDS No.41-1104), which were marked with ♦ (Fig. 7a-2), and the others were collected from Bi_2O_3 and ITO substrate. Fig. 7b shows the SEM images of the Bi_2O_3/Ag_2O hybrid thin films. The SEM image presented two kinds of nanoparticles, the larger particles are Bi_2O_3 nanoparticles (low-magnification SEM (inset) image illustrates Bi_2O_3 nanoparticles) and the smaller particles are the Ag_2O nanoparticles. The SEM images show that the silver oxide (Ag_2O) nanoparticles are distributed over the bismuth oxide (Bi_2O_3) nanoparticles uniformly.

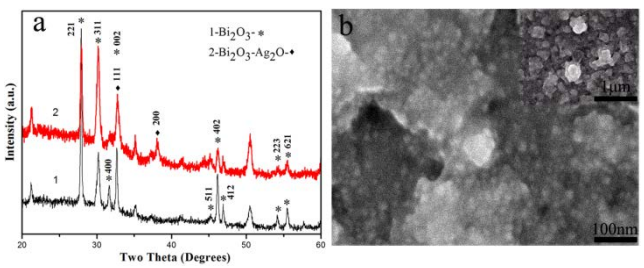

Fig. 7 (a) XRD patterns of pure Bi_2O_3 thin film (1) and Bi_2O_3/Ag_2O thin film (2). (b) High-magnification SEM image and low-magnification SEM image (inset) of Bi_2O_3/Ag_2O composite thin films.

We adopted a conventional three-electrode set-up to evaluate the thin film photovoltaic performance with an electrochemical workstation, by using the 'Amperometric i-t Curve' technique. The saturated calomel electrode (SCE) served as a reference electrode a platinum wire was used as an auxiliary electrode, and the pure Bi_2O_3 or Bi_2O_3/Ag_2O composite thin films on ITO conductive glass substrate were set as working electrodes. The active area of the working electrode was about 1.0 cm^2. A Uv light (the input power is 6W) was employed as a light source. Fig. 8 plots the photocurrent density curves of pure Bi_2O_3 (a) and Bi_2O_3/Ag_2O composite thin films (b) respectively. As Uv light on, the photocurrent increased immediately in both curves, it was important to note that the peak photocurrent density of the Bi_2O_3/Ag_2O hybrid thin films is an order of magnitude higher than that in the pure Bi_2O_3 thin film (the left y-axis value start from -0.1 to 6). The increase of the photocurrent density attributed to the formation of Bi_2O_3/Ag_2O p-n junction. In this hybrid thin film, the light is absorbed by Bi_2O_3/Ag_2O active layer, and electron-hole pairs generated. Then the electron-hole pairs diffuse to the Bi_2O_3/Ag_2O interface where the pairs can be separated and the electron and holes transport by Bi_2O_3 and Ag_2O respectively. The schematic diagram of such a process has been shown in Fig. 6. Driven by the electric filed force in the Bi_2O_3/Ag_2O p-n junction, the electron-hole pairs can be separated more effectively than a single Bi_2O_3 semiconductor thin film.

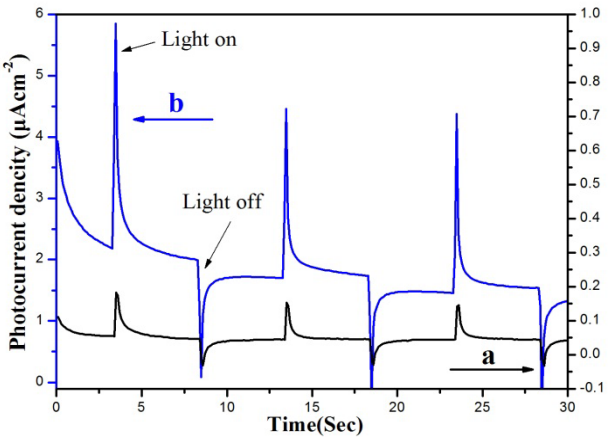

Fig. 8 Photocurrent densities of bare Bi_2O_3 thin film (a) and Bi_2O_3/Ag_2O composite thin films (b) measured under 6W Uv lamp in 0.1M Na_2SO_4 solution.

Conclusions

In summary, we have demonstrated a simple, controllable, room temperature, solvent-free, low-cost, dry chemical strategy to *in-situ* fabricate silver oxide (AgO and Ag_2O) thin films directly on ITO surface. The effects of relative humidity, temperature, and choice of substrate were determined for the formation of silver oxide thin films. We found that relative humidity plays a critical role in determining the composition of the final products. Pure AgO could be synthesized directly on ITO surfaces when the relative humidity was less than 40%, while pure Ag_2O thin films could only be obtained when the relative humidity was higher than or equal to 65%. The advantageous crystal growth faces of Ag_2O thin films could be

well controlled using the method we developed by choosing appropriate substrate. A possible mechanism for the formation of AgO and Ag_2O was proposed. Importantly, novel Bi_2O_3/Ag_2O heterojunction thin films were prepared for the first time as a photoelectrode for PV detection. The Bi_2O_3/Ag_2O heterojunction thin film electrode exhibited higher photovoltaic performances than the pure Bi_2O_3 thin film, which is attributed to the formation of the p-n heterojunction at the interface between n-type Bi_2O_3 and p-type Ag_2O. In the future, this novel Bi_2O_3/Ag_2O heterojunction thin film could be applied in bulk heterojunction (BHJ) solar cells which consist of an donor-acceptor (D-A) structure.

Acknowledgements

This work was supported by the National Natural Science Foundation of China (21273192, 61204009), Innovation Scientists and Technicians Troop Construction Projects of Henan Province (Grant No. 144200510014), and the Program for Science & Technology Innovation Talents in Universities of Henan Province (2011HASTIT029).

Notes and references

[a] *Key Laboratory for Micro-Nano Energy Storage and Conversion Materials of Henan Province, Institute of Surface Micro and Nano Materials, Xuchang University, Henan 461000, P. R. China. Fax: +86-374-2968988; Tel: +86-374-2968988; Email:zhengzhi99999@gmail.com*

[b] *The College of Chemistry and Molecular Engineering, Zhengzhou University, Henan 450001, P. R. China. E-mail: houhongw@zzu.edu.cn.*

1 J. J. Loferski, *J. Appl. Phys.* 1956, **27**, 777.
2 W. J. Danaher and L. E. Lyons, *Nature* 1978, **271**, 139.
3 H. Katagiri, K. Jimbo, K. Oishi, M. Yamazaki, H. Araki and A. Takeuchi, *Thin Solid Films*, 2009, **517**, 2455.
4 L. Shi, C. J. Pei, Y. M. Xu, and Q. *J.* Li, *Am. Chem. Soc.* 2011, **133**, 10328.
5 Y. Ida, S. Watase, T.Shinagawa, M. Watanabe, M. Chigane, M. Inaba, A. Tasaka and Izaki, *M. Chem. Mater.* 2008, **20**, 1254.
6 M. B. Zhou, W. T. Wei, Y. X. Xie, Y. Lei, J. H. Li, *J. Org. Chem.* 2010, **75**, 5635.
7 N. Yamamoto, S. Tonomura, T. Matsuoka and H. Tsubomura, *Jpn. J. Appl. Phys.* 1981, **20**, 721.
8 L. A. Peyser, A. E. Vinson, A. P. Bartko, R. M. Dickson, *Science* 2001, **291**, 103.
9 A. P. Karpinski, B. Makovetski, S. J. Russell, J. R. Serenyi, D. C. *J.* Williams, *Power Sources* 1999, **80,** 53.
10 L. H. Tjeng, M. B. J. Meinders, J. van Elp, J. Ghijsen and G. A. Sawatzky，*Phys. Rev. B*, 1990, 41, 3190
11 A. A. Noyes and D. A. Kohr, *J. Am. Chem. Soc.* 1902, **24**, 1141.
12 L. M. Lyu, W. C. Wang, and M. H. Huang, *Chem. Eur. J.* 2010, **16**, 14167.
13 Z. J. Yan, R. Q. Bao And B. C. Douglas, *Langmuir* 2011, **27**,851.
14 B. J. Murray, Q. Li, J. T. Newberg, E. J. Menke, J. C. Hemminger and R. M. Penner, *Nano Lett.*, 2005, **5,** 2319**.**
15 C. Y. Dong, D. S. Shang, L. Shi, J. R. Sun, B. G. Shen, F. Zhuge, R.W. Li and W. Chen, Appl. Phys. Lett., 2011, **98**, 072107
16 Y. Ida, S. Watase, T. Shinagawa, M. Watanabe, M. Chigane, M. Inaba, A. Tasaka, Izaki, *Cryst. Growth Des.*, 2013, **13**, 52.
17 Y. Chiu, U. Rambabu, M. H. Hsu, H. P. D. Shieh, C. Y. Chen and H. H. Lin, *J. Appl. Phys.*, 2003, **94**, 1996.
18 G. I. N. Waterhouse, G. A. Bowmaker, J. B. Metson, *Appl. Surf. Sci.*, 2001, **183**, 191.
19 R. Wiesinger, I. Martina a, Ch. Kleber, M. Schreine, *Corrosion Science*, 2013, **77**, 69.
20 L. Li, J. C. Yang, T. K. Minton, *J. Phys. Chem. C* 2007, **111**, 6763.
21 G. Q. Max. Lu, P. Pichat, *Photocatalysis Water Purification from Fundamentals to Recent Applications, Wiley*, 2013, **1**, 9.
22 P. Wardman, *J. Phys. Chem. Ref.*, 1989, **18**, 1637.
23 J. F. Weaver and G. B. Hoflund, *Chem. Mater.* 1994, **6**, 1693.
24 Q. Li, C. Zou, L. Zhai, L. J. Zhang, Y. Yang, X. Chen, S. M. Huang, *CrystEngComm*, 2013, **15**, 1806
25 J. F. Weaver and G. B. Hoflund, *J. Phys. Chem.* 1994, **98,** 8519.
26 G. B. Hoflund and Z. F. Hazos, *Phys. Rev. B*, 2000, **62**, 11126.
27 S. J. Hong, S. Lee, J. S. Jang and J. S. Lee, *Energy Environ. Sci.*, 2011, **4,** 1781.